Advanced Composite Materials

ISSN: 0924-3046 (Print) 1568-5519 (Online) Journal homepage: http://www.tandfonline.com/loi/tacm20

Enhanced geometric model for numerical microstructure analysis of plain-weave fabric-reinforced composite

Piotr Kowalczyk

To cite this article: Piotr Kowalczyk (2015) Enhanced geometric model for numerical microstructure analysis of plain-weave fabric-reinforced composite, Advanced Composite Materials, 24:5, 411-429, DOI: 10.1080/09243046.2014.898439

To link to this article: http://dx.doi.org/10.1080/09243046.2014.898439

Published online: 25 Mar 2014.

Advanced Composite Materials, 2015
Vol. 24, No. 5, 411–429, http://dx.doi.org/10.1080/09243046.2014.898439

Enhanced geometric model for numerical microstructure analysis of plain-weave fabric-reinforced composite

Piotr Kowalczyk*

Institute of Fundamental Technological Research, Polish Academy of Sciences, Pawińskiego 5b, 02-106 Warsaw, Poland

(*Received 3 December 2013; accepted 10 February 2014*)

Although there have been several numerical models used by different authors to model microstructural behaviour of a woven fabric-reinforced composite ply, they all suffer from geometric simplifications that may affect their validity or at least accuracy of results. This paper presents an enhanced model of a representative volume element RVE of this kind of composite with the plain-weave fabric pattern. Many important simplifications are overcome while the mathematical description remains simple. A dedicated FE mesh generator allows to reproduce all geometric details in the computational model. Computational examples of homogenization of orthotropic elastic constants illustrate application of the model.

Keywords: geometric modelling; fabric-reinforced composite; plain-weave fabric; homogenization; finite element analysis

1. Introduction

Composite fibre-matrix laminates enjoy increasing interest in automotive, aviation and shipbuilding industries as high-performance materials with advantageous mechanical and chemical properties. This increasing interest is followed by the need for their reliable numerical models that allow to predict their mechanical properties at different modelling scales.

Composite laminate consists of several laminae of fibre-matrix pre-impregnated plies stacked on each other and moulded together to form a multilayer sandwich-like plate. Apart from unidirectional fibre-matrix prepregs, woven fabric-reinforced plies are widely used as laminae in production of composite laminates. Woven fabrics are appreciated for their low manufacturing costs, better durability in handling and easy formability, especially in doubly curved laminate components.[1–3] They consist of two families of parallel yarns, interlaced usually at right angle and immersed in matrix. The yarns are made of multiple parallel fibres, bonded to each other by the same matrix material that fills the space between them and around the yarns. Due to yarn curvatures (undulation), woven fabric plies have lower in-plane stiffness and strength than analogous unidirectional fibre plies in the fibre axis direction.[4] Among several possible weave patterns (Figure 1), the simplest plain-weave type is most commonly applied in industrial applications.

*Email: Piotr.Kowalczyk@ippt.pan.pl

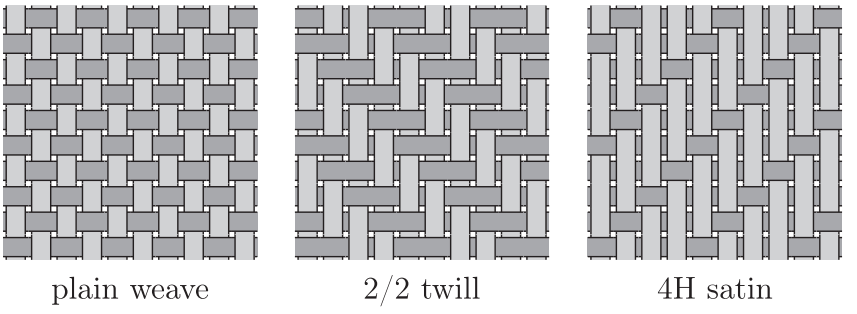

Figure 1. Examples of geometric patterns in woven fabric plies.

Numerical models of mechanical behaviour of composite laminates are mainly based on the classical laminate theory (CLT) [5] in which the laminate is treated as a layered Kirchhoff–Love shell whose layers (laminae) are considered homogeneous, have constant thickness and remain in the plane stress state. The lamina's material is typically assumed orthotropic with one of the principal directions normal to the layer. Extension of this model towards the Reissner–Mindlin kinematical hypothesis [5,6] results in the appearance of transversal shear stresses and strains in each lamina. In view of these facts, homogenized mechanical properties of each lamina are crucial data needed to use this model in practice.

There have been several papers published on this issue regarding woven fabric materials, dating back to works of Ishikawa and Chou [7,8], through following contributions, e.g. [9–24]. Particularly, the case of plain-weave geometry has been extensively researched in e.g. [1–3,25–33]. The main idea is to define a representative volume element (RVE) and to derive its macroscopic mechanical properties by correctly determining its microscopic deformation and stress fields under certain loads.

In the case of plain-weave fabric-reinforced composite ply, whose idealized scheme is shown in Figure 2(a), the natural choice is the repeatable cell shown in Figure 2(b). It is characterized by a few geometric parameters and material parameters of the composite constituents: matrix (usually assumed isotropic) and yarns. If the twist of fibres in yarns is not significant, each yarn may be treated as a unidirectional tow featuring transversely isotropic properties with the principal direction aligned with the curved yarn axis.

There are two approaches used to determine the stress and strain fields in RVE – analytical and numerical. In the first one, the local displacement and/or temperature field is approximated with e.g. linear function [9,11] or the Fourier series.[33] In the other, it is approximated by the finite element analysis (FEA).[3,15,25,27,29,32] A comprehensive review of both analytical and numerical research on mechanical properties of woven fabric composites up to 2007 can be found in [34].

In all the cases, strict assumptions about the constituents' geometry and periodic boundary conditions in the repeatable RVE are necessary. It has to be noted that, although extended research devoted to this subject has been done in the recent 20 years, the geometric assumptions in the exploited RVE models suffered from substantial simplifications. Some authors [10,31] have neglected geometric details of yarns and replaced the 3-D modelling approach with a concept of sub-element layers. But even in the papers where shapes of the microstructure components' and their interfaces are

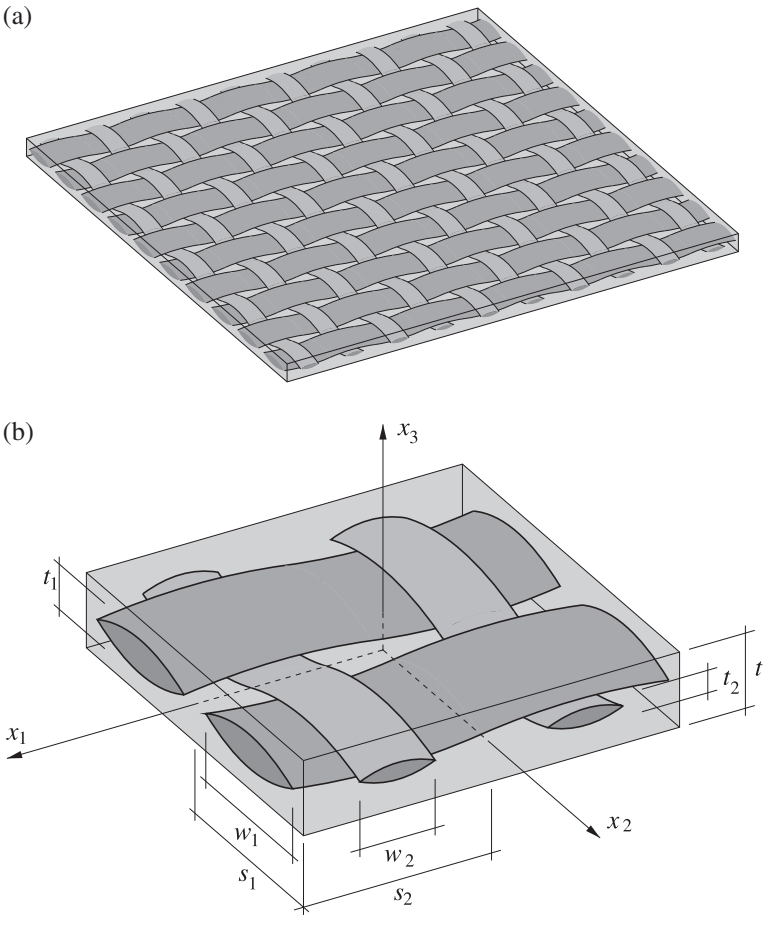

Figure 2. Plain-weave fabric composite lamina, (a) geometric model, (b) a representative volume element.

discussed in detail,[15,25,26,30,33] some important features have been treated in a simplified manner or neglected.

Yarn cross-sections are sometimes assumed elliptic,[11,31,35–37] but in view of available microphotographs of woven fabric composite microstructures (see e.g. [33] for carbon,[38] for aramid and [39,40] for glass reinforcement fabrics), most authors tend to rather model their shape as lenticular, with sinusoidal or circular arch-shaped boundary.[3,9,15,25–27,30,33,41] Moreover, geometric considerations lead to a conclusion that the lenticular cross-section is not symmetric [15,26,30,33] and its shape varies along the yarn length (section is generally flattened at the contact interface with an interlacing yarn and bulged on the opposite side), however, this feature is neglected in many geometric models.

To define yarn surfaces, the yarn cross-section has to be moved along the curved yarn axis. Usually, simple translation along a sinusoidal (or circular arch-shaped) path is assumed. This definition does not preserve constant cross-section area of yarns (indeed, it is constant in all ‘vertical’ cross-section planes, but considering cross-sections locally orthogonal to the yarn axis, see Figure 3, the higher the local undulation

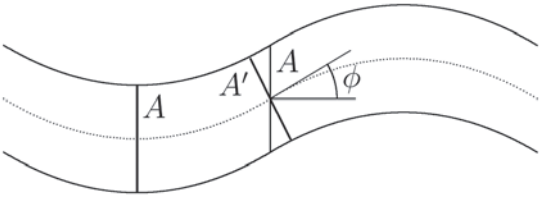

Figure 3. Variable cross-section area in a classical yarn model.

angle ϕ, the smaller the cross-section area $A' < A$ is). This seems non-physical, especially in case of high yarn aspect ratios (t_i/w_i), because the number of fibres in each yarn cross-section is the same, thus their summaric cross-section area measured orthogonally to the fibre axis (which is approximately parallel to the yarn axis) should remain the same in all cross-sections. This might be justified if fibres underwent significant shear deformations in the undulated yarn but these are rather negligible. On the other hand, it is argued that, in cross-sections corresponding to significant values of ϕ, fibre packing density is higher than elsewhere and that local decrease of the yarn cross-section area corresponds to lower amount of matrix material. This does not seem justified either, since the fibre density in yarns is usually high, close to its highest geometrically allowable value, hence the assumption of its increased value in some cross-sections is questionable. Besides, the increased fibre density should result in higher local macroscopic yarn stiffness; it is noteworthy that this fact was not taken into account in the cited computational models.

There is a variety of different approaches to modelling of yarn-to-yarn interface (two striped surface patches within zone I in Figure 4), as well as the matrix `eye' at the intersection of inter-yarn spaces (zone III in Figure 4). As it can be seen, the adjacent yarn surfaces do not remain in full contact. In fact, contact occurs only in the neighbourhood of central planes of both the yarns. Elsewhere, there is a thin gap

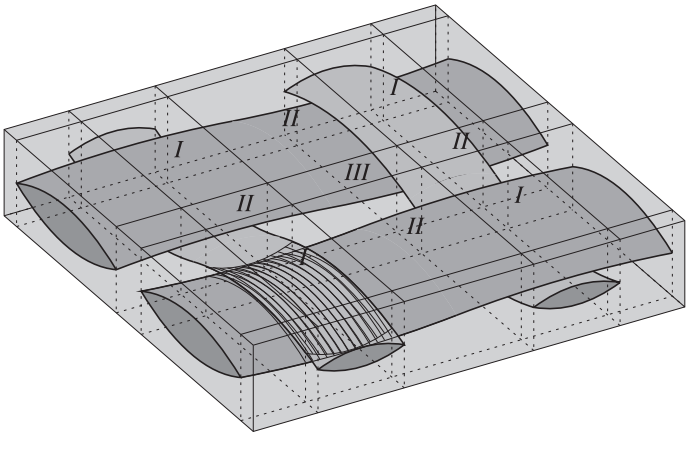

Figure 4. RVE for plain-woven fabric composite lamina – geometry details; zone I contains interlace of two yarns, zone II contains bridge segments of yarns (between intersections) and zone III – the matrix space between yarns.

between the surfaces. The only case when the gap vanishes is when no horizontal inter-yarn spaces in both the yarn families exist, i.e. $w_1 = s_1$ and $w_2 = s_2$ (no zones II and III). In some of the cited models,[27] the authors limit themselves to just this special case, in some other,[28,30] geometry of yarns is initially deformed so that they remain in full contact within the interlace zone I. The latter assumption may only be justified for very flat, wide yarns. In [25], an artificial finite thickness matrix layer is introduced between the contacting interfaces. In [15], the inter-yarn gap is assumed filled with matrix and its geometry is investigated in detail, however, the geometric model refers to only the satin-weave fabric pattern (where the matrix gap is even more evident than in the plain-weave fabrics). In [1,3,14,32,37], the interface geometry is modelled with no simplifications, however, the authors consider only the textile component of the composite, neglecting matrix.

The objective of this paper is to present a geometric model of the RVE for plain-weave woven fabric laminae that is free from the above-mentioned simplifying assumptions and easy to use in numerical homogenization analysis. Exact geometry of yarns and matrix-filled zones is defined, including details of matrix space (zone III), as well as gaps between interlacing yarn surfaces (striped patches in zone I in Figure 4). A dedicated finite element mesh generator has also been written, so that correct hexahedral meshes of required density can be obtained for different values of geometric parameters.

2. Geometric model of the RVE

2.1. Analytical description

Woven fabric composite ply has complex 3D geometry. Yarns form two families arranged in two orthogonal directions: x_1 (warp yarns) and x_2 (weft yarns), see Figure 2. Yarns of these families are mutually woven around each other forming fabric in which each yarn is multiply undulated and contacts the others at the internal surface of each undulation. Contact does not usually occur at the entire yarn surface (more strictly – the rectangular part of the surface that `meets' the analogous part of the interlacing yarn surface; see two adjacent striped areas in Figure 4); there is rather a thin, sharp-edged gap between the contacting yarns. This space is assumed filled with matrix (although other assumptions may be alternatively made here). The entire remaining space around yarns is also filled with matrix that extends up to $x_3 = \pm\frac{t}{2}$, i.e. to the upper and lower surfaces of the lamina.

All interfaces of microstructure constituents (yarns and matrix) are assumed perfectly glued in the model. Again, other assumptions may also be made regarding the interface contact conditions.

In this study, the mathematical description of yarn geometry is based on the following fundamental assumptions.

(1) The yarn in its actual shape is transformation image of a parent rectangular prism depicted in Figure 5(a). Value ranges of the parent coordinates are $\xi_2 \in \left[-\frac{1}{2}, \frac{1}{2}\right]$, $\xi_3 \in \left[-\frac{1}{2}, \frac{1}{2}\right]$, while ξ_1 is generally infinite but – limiting ourselves to a single RVE – we can set its limits as approximately[1] $\xi_1 \in [-1, 1]$. Coordinates of each material point of the yarn (x_1, x_2, x_3) are thus parametric functions of (ξ_1, ξ_2, ξ_3), see Figure 5(b). The transformation is reversible except for the yarn side edges ($\xi_2 = \pm\frac{1}{2}$) where singularity occurs.

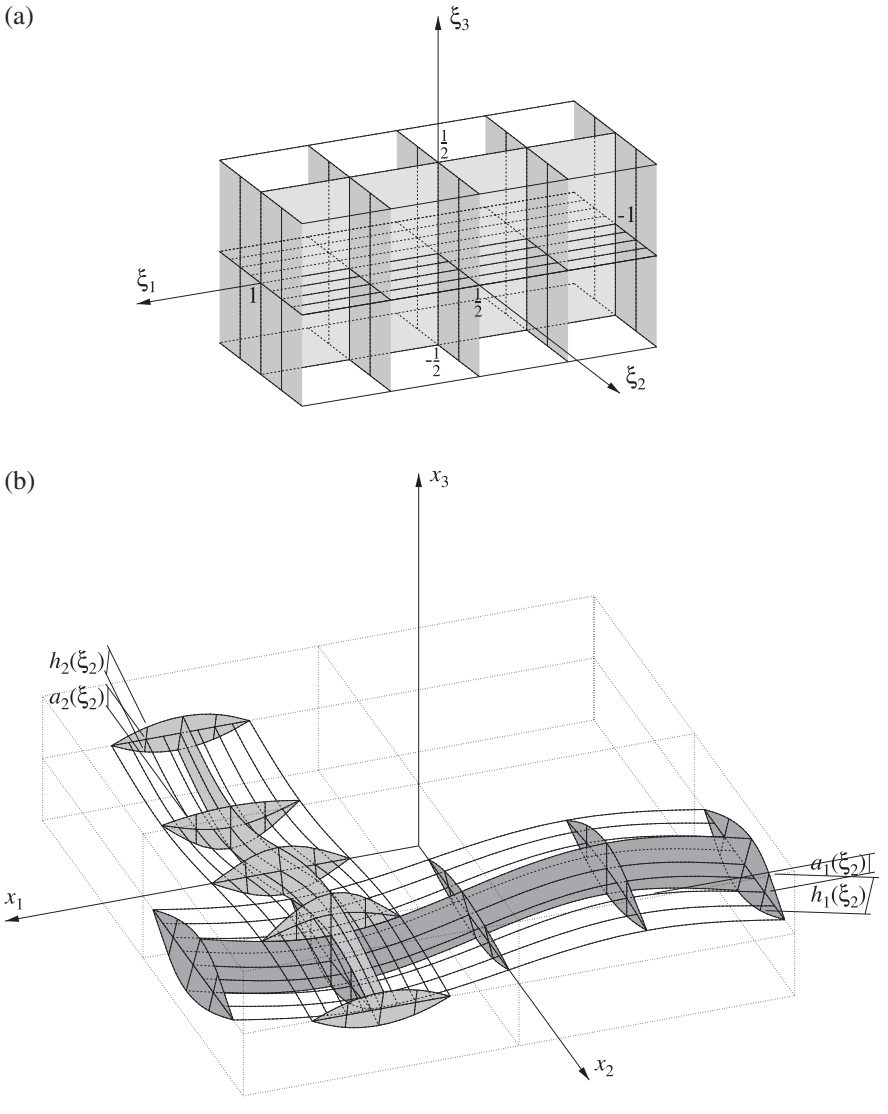

Figure 5. Parent (a) and actual (b) configuration of yarns in RVE. Shaded are the central strip ($\xi_2 = 0$) and the cross-sections perpendicular to undulated central lines ($\xi_1 = \text{const}$). Warp yarn sections are shaded in darker gray.

(2) The central plane axial lines ($\xi_3 = 0$, $\xi_2 = \text{const}$) in the parent configuration are transformed to sinusoidal lines described by the following equations

$$x_1 = \xi_1 s_2, \quad x_2 = \frac{s_1}{2} + \xi_2 w_1 = \text{const}, \quad x_3 = -a_1(\xi_2)\ \sin(\pi\xi_1) \tag{1}$$

for the warp yarn and

$$x_1 = \frac{s_2}{2} + \xi_2 w_2 = \text{const}, \quad x_2 = \xi_1 s_1, \quad x_3 = a_2(\xi_2)\ \sin(\pi\xi_1) \tag{2}$$

for the weft yarn.[2] The coefficients a_1 and a_2 are undulation parameters of each line. For the central line ($\xi_2 = 0$) they equal $a_1 = \frac{1}{2}t_2$ (warp yarn) and $a_2 = \frac{1}{2}t_1$ (weft yarn), respectively. For other ξ_2, values of a_1 and a_2 will be derived further.

(3) Each vertical segment in the parent configuration, $\xi_3 \in \left[-\frac{1}{2}, \frac{1}{2}\right]$, perpendicular to such a central axial line at the point (ξ_1, ξ_2, 0) remains in the actual configuration straight, perpendicular to the sinusoid line given by Equations (1) or (2), its centre lies on the sinusoid line and its height h_i, constant along ξ_1, equals

$$h_i(\xi_2) = t_i \ \cos(\pi\xi_2) \tag{3}$$

(with $i = 1$ for the warp yarn and $i = 2$ for the weft yarn). In other words, a rectangular cross-section $\xi_2 = \text{const}$ of the parent prism corresponds in the real yarn to a curved constant width strip in the plane $x_2 = \text{const}$ (for warp yarns) or $x_1 = \text{const}$ (for weft yarns) whose central line is a sinusoid given by Equations (1) or (2) and whose width h_i depends on ξ_2 according to Equation (3). For the warp yarn, these assumptions can be expressed with the following parametric equations

$$\begin{aligned} x_1(\xi_1, \xi_2, \xi_3) &= x_1(\xi_1, \xi_2, 0) - \xi_3 h_1 \sin\phi, \\ x_2(\xi_1, \xi_2, \xi_3) &= x_2(\xi_1, \xi_2, 0), \\ x_3(\xi_1, \xi_2, \xi_3) &= x_3(\xi_1, \xi_2, 0) + \xi_3 h_1 \cos\phi \end{aligned} \tag{4}$$

where x_i (ξ_1, ξ_2, 0) are given by Equations (1), $h_1 = h_1(\xi_2)$ is given by Equation (3) and $\phi(\xi_1, \xi_2)$ is the undulation angle, i.e. the angle whose tangent $\tan\phi$ equals the directional slope $\partial x_3/\partial x_1$ of the parametric surface defined by Equations (1). Substituting $(1)_1$ to $(1)_3$ and denoting $b_1(\xi_1, \xi_2) = \tan\phi$ and $c_1(\xi_1, \xi_2) = \cos\phi$, we obtain

$$b_1 = \frac{\partial x_3(\xi_1, \xi_2, 0)}{\partial x_1} = -\frac{\pi a_1(\xi_2)}{s_2} \ \cos(\pi\xi_1), \quad c_1 = \frac{1}{\sqrt{1 + b_1^2}} \tag{5}$$

and rewrite Equations (5) as

$$\begin{aligned} x_1 &= \xi_1 s_2 - \xi_3 h_1 b_1 c_1, \\ x_2 &= \frac{s_1}{2} + \xi_2 w_1, \\ x_3 &= -a_1(\xi_2) \ \sin(\pi\xi_1) + \xi_3 h_1 c_1. \end{aligned} \tag{6}$$

Analogously, we derive for the weft yarn

$$\begin{aligned} x_1 &= \frac{s_2}{2} + \xi_2 w_2, \\ x_2 &= \xi_1 s_1 - \xi_3 h_2 b_2 c_2, \\ x_3 &= a_2(\xi_2) \ \sin(\pi\xi_1) + \xi_3 h_2 c_2. \end{aligned} \tag{7}$$

with $h_2 = h_2(\xi_2)$ given by Equation (3) and

$$b_2 = \frac{\partial x_3(\xi_1, \xi_2, 0)}{\partial x_2} = \frac{\pi a_2(\xi_2)}{s_1}\cos(\pi\xi_1), \quad c_2 = \frac{1}{\sqrt{1+b_2^2}}. \tag{8}$$

(4) The only relationships needed to complete the transformation Equations (7) and (8) are the distributions $a_i(\xi_2)$. Note that their values are already known at $\xi_2 = 0$, i.e. one can determine the 'central strip' of each yarn (image of the parent rectangular cross-section at $\xi_2 = 0$, shaded in Figure 5). It is now assumed that all strips of the weft yarn contact the warp yarn at the upper edge of its central strip. Similarly, all strips of the warp yarn contact the weft yarn at the lower edge of its central strip. This condition allows to determine distributions of $a_i(\xi_2)$ in Equations (7) and (8) for both yarns. For instance, to compute a_2 for a given $\xi_2 = c$ for the weft yarn, one needs to consider a point on its lower surface being the image of $(\xi_1, \xi_2, \xi_3) = \left(\frac{1}{2}, c, -\frac{1}{2}\right)$. Its actual coordinates are $x_1 = \frac{s_2}{2} + cw_2$, $x_2 = \frac{1}{2}s_1$ and $x_3 = a_2 - \frac{1}{2}h_2$. According to our assumptions, this is the contact point of the two yarns. The adjacent point of the warp yarn lies at the upper edge of its central strip and must have the same coordinates. Thus, one needs to find the point at this edge of the warp yarn whose coordinate x_1 equals $\frac{s_2}{2} + cw_2$ (this is an inverse problem of Equation (7)), compute its coordinate x_3, and realize that for the weft yarn there must be $a_2 = x_3 + \frac{1}{2}h_2$. Analogous algorithm can be formulated to compute values of a_1 for the warp yarn. Unfortunately, the relationships $a_i(\xi_2)$ cannot be expressed with closed-form formulae and they are rather derived for given values of ξ_2 in numerical iterations.

The above conditions are complete and allow to determine actual positions of all yarn material points, in particular their surface points.

In the presented model, lines that fulfil the conditions $\xi_2 = \text{const}$, $\xi_3 = \text{const}$ in the parent configuration correspond to curved axes of individual fibres in yarns. In the case of $\xi_3 = 0$ they are given with Equations (1) and (2). Note that these lines are not parallel to each other; thus, the perpendicular segments described in the condition 3 are neither. This means that a planar cross-section $\xi_1 = \text{const}$ in the parent prism, when transformed to the actual yarn cross-section, is generally not planar any more (although it is ruled by straight lines). This may be considered a violation of our previous assumption that individual fibres in yarns are laid parallelly (which allows to assume the yarns to be transversely isotropic and to employ the parametric constitutive equations for UD tows). It must be noted, however, that for the assumed model geometry (small thickness-to-width ratio of yarns) such a non-parallel deviation is insignificant and its effects will be neglected in further discussion. Besides, to accommodate these small deviation from parallel yarn layout, the principal axis of transverse isotropy in yarns will be assumed parallel to the lines given by Equations (1) and (2) in each yarn section point.

The geometric model described above preserves constant cross-section area of yarns measured perpendicularly to the yarn axes. Moreover, it allows yarns to be shaped freely – each fibre in the yarn forms a sinusoid whose undulation is only constrained by neighbouring fibres and by presence of intersecting yarns. This results e.g. in cyclic asymmetry of yarn cross-sections at intersections with other yarns, observed in microphotographic images [33] and frequently disregarded in geometric models. Consequently, the yarn surfaces at their contact interface are described realistically, with the

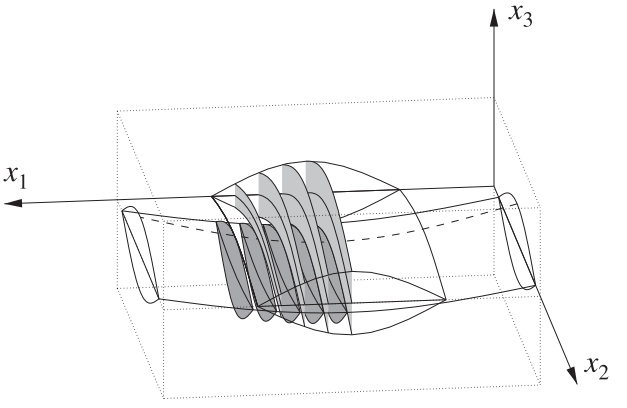

Figure 6. Yarn-to-yarn contact zone shown on cross-sections $x_1 = \text{const}$ according to the presented geometric equations. Visible are sharp-edged curvilinear gaps between yarns; full contact occurs along the central strip edges only.

natural gap that forms between them. Figure 6 shows a number of cross-sections of the RVE quarter made with parallel surfaces $x_1 = \text{const}$. Yarn sections are shaded. One can see that full contact between yarns occurs along the central strip edges only ($\xi_2 = 0$, $\xi_3 = \frac{1}{2}$ for the warp yarn – dashed line in Figure 6, and $\xi_2 = 0$, $\xi_3 = -\frac{1}{2}$ for the weft yarn – solid line in the most right cross-section in Figure 6). In the remaining area, a thin sharp-edged gap between yarns is visible.

2.2. *Material properties*

Material properties of the microstructure constituents are generally anisotropic and it is necessary to define principal directions orientation in material points of the geometric model. For elastic stiffness **C**, described by tensorial coefficient of the 4th rank, local components of this material tensor in the Cartesian coordinate system (x_1, x_2, x_3) are denoted by C^{m}_{ijkl} for matrix and C^{y}_{ijkl} for yarns, respectively.

Matrix is usually assumed isotropic. For yarns, the assumption of orthotropy (at least transversal isotropy) has to be generally made. In the geometric model presented, the local orientation of principal axes of orthotropy is assumed to coincide with axes (ξ_1, ξ_2, ξ_3) which are approximately orthogonal in the actual configuration of RVE. Thus, components of the material stiffness tensor will be expressed as

$$C^{\mathrm{y}}_{ijkl} = R_{ip}R_{jq}R_{kr}R_{ls}\ C^{\mathrm{y\ loc}}_{pqrs}, \tag{9}$$

where the components superscribed by y loc are known material constants of yarns in their natural coordinate system defined by local orientation if fibres while R_{ip} are components of the local rotation matrix, i.e. normalized derivatives $\mathrm{d}x_i/\mathrm{d}\xi_p$.

An important property of fibre-matrix composites is the fibre volume fraction $\beta = V^{\mathrm{f}}/V$. This depends on the fibre packing density in yarns and relations between yarn volumes and the total composite volume. It is assumed that warp and weft yarns are UD fibre-matrix tows with constant fibre volume fractions $\beta^{\mathrm{y\ warp}}$ and $\beta^{\mathrm{y\ weft}}$, respectively, (usually $\beta^{\mathrm{y\ warp}} = \beta^{\mathrm{y\ weft}} = \beta^{\mathrm{y}}$). Thus,

$$\beta = \frac{1}{V}(\beta^{\text{y warp}} V^{\text{y warp}} + \beta^{\text{y weft}} V^{\text{y weft}}). \tag{10}$$

For the model RVE (Figure 2), the total volume is $V = 4s_1 s_2 t$. Volumes of yarns, $V^{\text{y warp}}$ and $V^{\text{y weft}}$, cannot be easily expressed analytically; they can be approximately determined, though, during the finite element mesh generation, described below.

2.3. *Finite element mesh*

To make the geometric model more handy in computational applications, a finite element mesh generator has been written to produce finite element meshes along with appropriate periodic boundary conditions defined for mesh nodes. Generated meshes consist of mainly 8-node brick elements. Only in the yarn-to-yarn interface zone, where the thickness of the matrix cushion is nearly zero, there are a few wedge elements

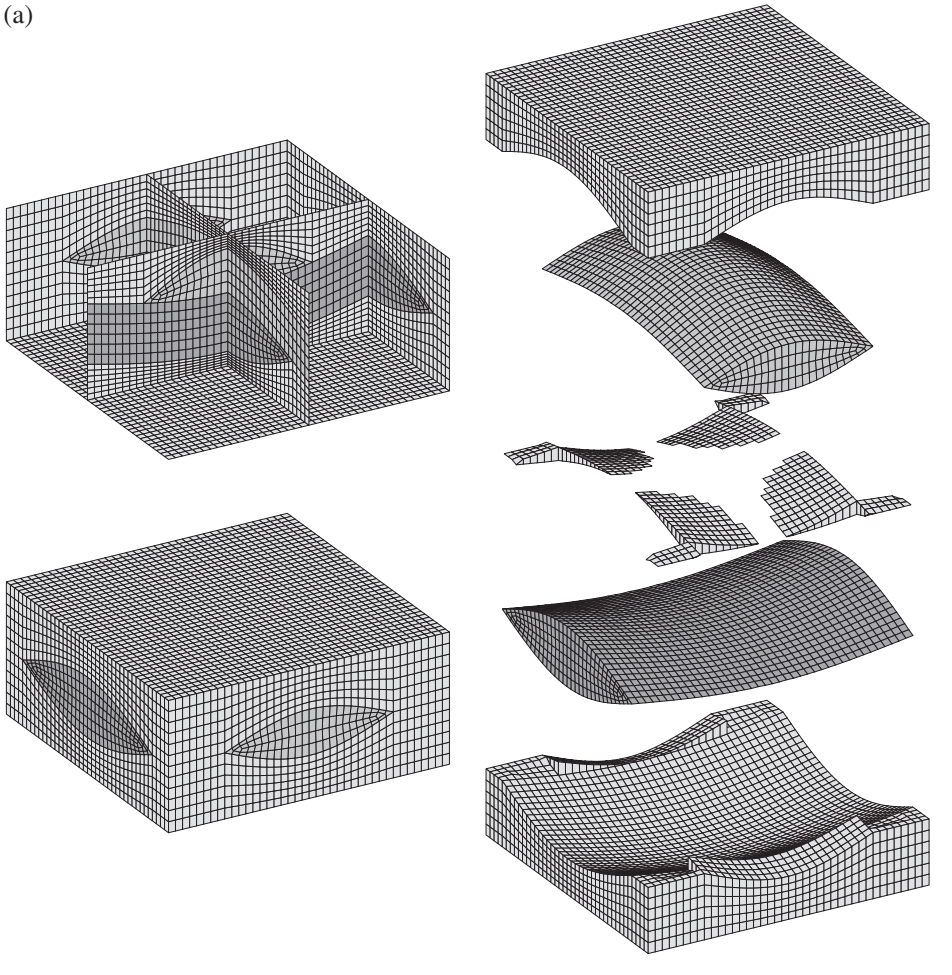

Figure 7. Representative volume element – examples of FE mesh; (a) $s_1 = s_2 = s$, $t = 0.45s$, $w_1 = 0.8s$, $w_2 = 0.6s$, $t_1/w_1 = {}_2/w_2 = 0.25$; (b) $s_1 = s_2 = s$, $t = 0.14s$, $w_1 = 0.8s$, $w_2 = 0.6s$, $t_1/w_1 = t_2/w_2 = 0.075$. (continued on the next page)

(b)

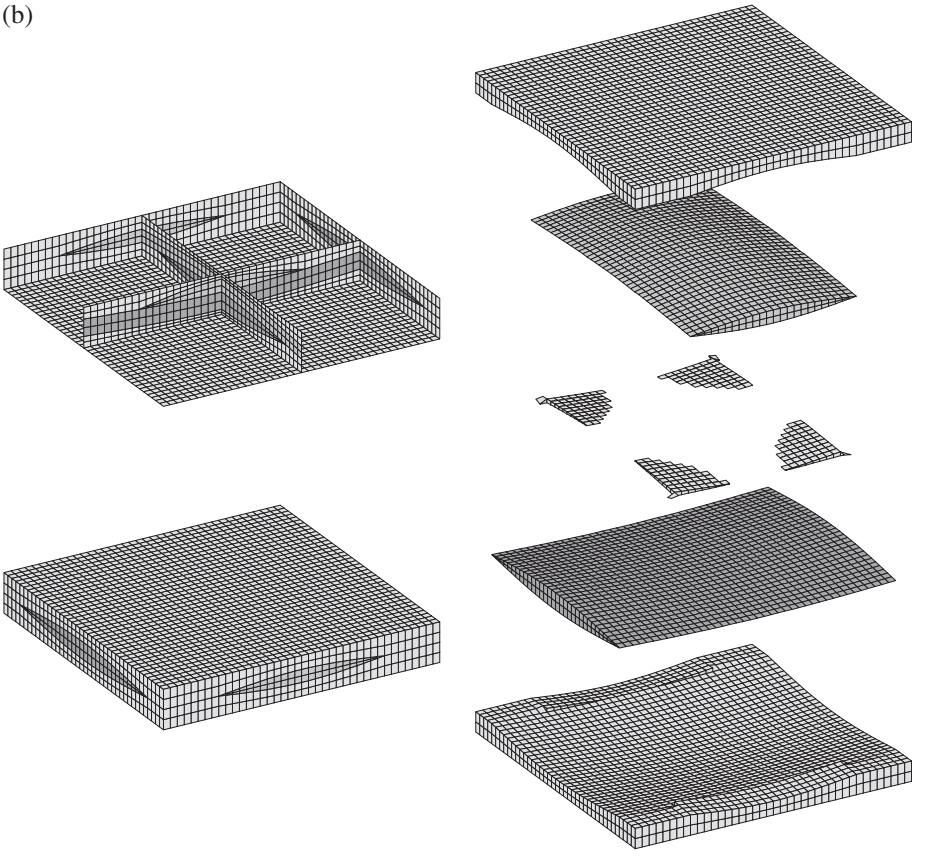

Figure 7. (*Continued*).

accompanied by a few degenerated bricks. Wherever the matrix layer thickness is less than 10% of the typical element size, the layer is neglected and the adherent elements of the neighbouring yarn surfaces are assumed in contact. Mesh density can be selected arbitrarily.

Figure 7 shows examples of finite element meshes for two different sets of geometric parameters of woven fabric composite. Main cross-sections and separated mesh layers for different microstructure components are shown in detail. The mesh generation algorithm ensures coincidence of surface nodes at the interfaces of microstructure constituents. This allows to impose various contact conditions at the interfaces, from full adhesion to slip contact with friction. In the following computational examples, full adhesion has been assumed there.

3. Application: numerical homogenization of elastic constants

As an example of application, the problem of numerical homogenization of elastic constants of the plain-weave woven fabric lamina has been solved. The problem formulation is classical. It will be shown that results obtained with the proposed geometry of the RVE cell correspond very well to experimental data, as well as to analytical results of other authors.

Finite element method has been used to solve a series of static analyses of a RVE cell with prescribed geometric parameters and material properties of the constituents (matrix and yarns). ABAQUS FE system [42] was employed in all reported analyses. Six deformation modes have been imposed on the FE cell model, each of them corresponding to the average state of strain in the cell in which only one of the strain components $\{\boldsymbol{\varepsilon}\} = \{\varepsilon_{11}, \varepsilon_{22}, \varepsilon_{33}, \varepsilon_{23}, \varepsilon_{31}, \varepsilon_{12}\}$ is non-zero while the others are zero. Having computed stress distributions in the cell for each of the strain states, we are able to determine six averaged stress components $\{\boldsymbol{\sigma}\} = \{\sigma_{11}, \sigma_{22}, \sigma_{33}, \sigma_{23}, \sigma_{31}, \sigma_{12}\}$ and, consequently, all 36 components of the 6×6 macroscopic elastic stiffness matrix of the composite, given by the formula

$$\{\boldsymbol{\sigma}\} = [\mathbf{C}]\ \{\boldsymbol{\varepsilon}\}. \tag{11}$$

No assumptions about anisotropy of $[\mathbf{C}]$ are made, however, it appears from the analysis results that it has an orthotropic form, with principal directions coincident with x_1, x_2, x_3, respectively:

$$[\mathbf{C}] = \begin{bmatrix} C_{11} & C_{12} & C_{13} & 0 & 0 & 0 \\ C_{12} & C_{22} & C_{23} & 0 & 0 & 0 \\ C_{13} & C_{23} & C_{33} & 0 & 0 & 0 \\ 0 & 0 & 0 & C_{44} & 0 & 0 \\ 0 & 0 & 0 & 0 & C_{55} & 0 \\ 0 & 0 & 0 & 0 & 0 & C_{66} \end{bmatrix}. \tag{12}$$

Deformation modes have been imposed by means of prescribed displacements at midpoints of the cell walls. Values of prescribed displacements for particular deformation modes are displayed in Table 1. The remaining nodes in the walls were subject to multipoint constraints. On side walls (i.e. those orthogonal to the axes x_1 and x_2), the constraints corresponded to periodic boundary conditions, imposed to ensure repeatability of the cell walls deformation in the neighbouring cells,

$$\begin{aligned} u_i(s_2, x_2, x_3) - u_i(s_2, 0, 0) &= u_i(-s_2, x_2, x_3) - u_i(-s_2, 0, 0), \\ u_i(x_1, s_1, x_3) - u_i(0, s_1, 0) &= u_i(x_1, -s_1, x_3) - u_i(0, -s_1, 0), \end{aligned} \tag{13}$$

Note that no other limitations on the wall deformation were produced by these conditions. On the upper and lower walls ($x_3 = \pm t/2$), plane stress conditions are typically assumed in analysis of this type, i.e. the deformation of the faces is allowed free. Here, however, the faces were treated in a different way. It has been assumed that the considered lamina is a part of a multilayer laminate composite shell, hence standard

Table 1. Prescribed displacements imposed on side midpoints for six deformation modes; $\epsilon << 1$ is an arbitrary strain level value.

No.	Average strain $\{\boldsymbol{\varepsilon}\}$	Imposed displacements
1	$\{\epsilon, 0, 0, 0, 0, 0\}$	$u_1(\pm s_2, 0, 0) = \pm\epsilon s_2$
2	$\{0, \epsilon, 0, 0, 0, 0\}$	$u_2(0, \pm s_1, 0) = \pm\epsilon s_1$
3	$\{0, 0, \epsilon, 0, 0, 0\}$	$u_3(0, 0, \pm\frac{t}{2}) = \pm\epsilon\frac{t}{2}$
4	$\{0, 0, 0, \epsilon, 0, 0\}$	$u_2(\pm s_2, 0, 0) = \pm\frac{1}{2}\epsilon s_2$, $u_1(0, \pm s_1, 0) = \pm\frac{1}{2}\epsilon s_1$
5	$\{0, 0, 0, 0, \epsilon, 0\}$	$u_3(\pm s_2, 0, 0) = 0$, $u_1(0, 0, \pm\frac{t}{2}) = \pm\epsilon\frac{t}{2}$
6	$\{0, 0, 0, 0, 0, \epsilon\}$	$u_3(0, \pm s_1, 0) = 0$, $u_2(0, 0, \pm\frac{t}{2}) = \pm\epsilon\frac{t}{2}$

free-surface plane stress conditions cannot be justified because the upper and lower face deformation of each lamina are constrained by deformation of the neighbouring laminae.[3] On the other hand, application of periodic conditions analogous to those imposed on the side walls (as it was done e.g. in [14]) corresponds to only a very impractical case when laminae are placed one on another in the same orientation and with zero tangential shift. This is, however, not the case – to the contrary, laminae are typically organized in such a way that their orientations (and sometimes also material properties) change from layer to layer. Deformation of the side face points of a lamina is thus locally constrained in a rather random way, depending on which parts of neighbouring lamina cells meet each other at a particular location. To overcome this problem, a sort

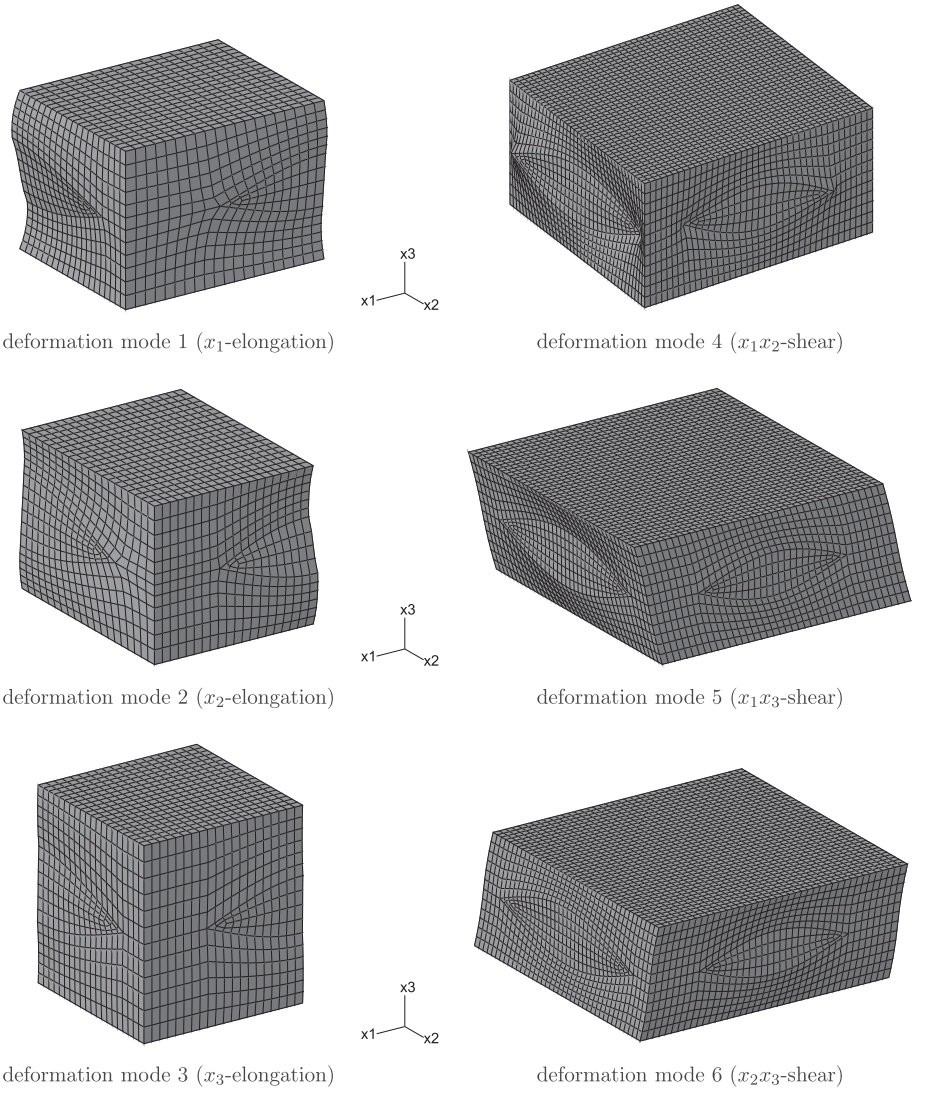

Figure 8. Representative volume element – deformation modes; symmetric quarters are only shown for the elongation modes.

of generalized plane strain assumption was enforced on the face deformation in this study. It was namely assumed that the faces $x_3 = \pm t/2$ remained plane and their deformation was uniform,

$$u_i(x_1, x_2, \pm\bar{t}) = u_i(0, 0, \pm\bar{t}) + \frac{x_1}{s_1}\, u_i(s_2, 0, 0) + \frac{x_2}{s_2}\, u_i(0, s_1, 0). \tag{14}$$

Figure 8 presents deformation modes of the cell FE mesh for a typical set of dimensionless geometric and material data: $E_p^{\mathrm{y}} = 1$, $E^{\mathrm{m}} = 0.01$, $E_t^{\mathrm{y}} = 0.16$, $G_{pt}^{\mathrm{y}} = 0.08$, $v^{\mathrm{m}} = 0.36$, $v_{pt}^{\mathrm{y}} = 0.25$ (i.e. $v_{tp} = 0.04$) $v_{tt}^{\mathrm{y}} = 0.20$, $s_1 = s_2 = 1$, $w_1 = 0.8$, $w_2 = 0.6$, $t_1 = 0.2$, $t_2 = 0.15$, $t = 0.45$ (subscripts p, t at anisotropic yarn data denote parallel and transversal directions, respectively). The strain level is $\epsilon = 0.001$ but displacements in the graphs are scaled by 250. One can see that the initially plane side walls of the RVE cell are visibly deformed out of their planes which results from significant differences between yarn and matrix material properties. Periodicity conditions are strictly preserved, though.

To validate the numerical model presented above, comparisons of FEA results were made to published material data and other numerical analyses of woven fabric composites and their laminates. Unfortunately, it is difficult to find comprehensive experimental results, including complete sets of measured elastic constants of both the constituents and the composite material. Available reports are limited to e.g. only few measured elastic constants, e.g. two longitudinal stiffness moduli in the warp and weft directions. On the other hand, it is much easier to find published results obtained with other numerical models. Thus, results of this study model are going to be compared with published data of both kinds.

FEA results strongly depend on mesh density. In the reported analyses, this parameter was selected at the level of 40 elements per cell width s. It was computationally verified that increase of this value by 50% makes the resulting elastic constants change by less than 1%.

Table 2. Comparison of this study results with those of [43] for e-glass/epoxy plain-weave composite.

Geometric data	Matrix data	Fiber data	Yarn data
$s_1 = s_2 = 0.67$ mm	$E^{\mathrm{m}} = 3.5$ GPa	$E^{\mathrm{f}} = 72$ GPa	$E_p^{\mathrm{y}} = 51.5$ GPa
$w_1 = w_2 = 0.62$ mm	$v^{\mathrm{m}} = 0.35$	$G^{\mathrm{f}} = 27$ GPa	$E_t^{\mathrm{y}} = 17.5$ GPa
$t_1 = t_2 = 0.05$ mm		$\beta^{v} = 0.70$	$G_{pt}^{\mathrm{y}} = 5.80$ GPa
$t = 0.10$ mm			$v_{pt}^{\mathrm{y}} = 0.31$
			$G_{tt}^{\mathrm{y}} = 6.60$ GPa

Woven fabric composite data	[43] exper.	[43] anal.	This study
$E_1 = E_2$ [GPa]	19.3	20.3	21.65
G_{12} [GPa]	–	3.7	3.88
$G_{13} = G_{23}$ [GPa]	–	–	2.82
v_{12}	–	0.23	0.166
$v_{13} = v_{23}$	–	–	0.373
β	0.42		0.412

Table 3. Comparison of this study results with those of [43] for carbon/epoxy plain-weave composite.

Geometric data	Matrix data	Fiber data	Yarn data, CCA model	Yarn data, FEA model
$s_1 = 1.14$ mm $s_2 = 1.14$ mm	$E^{m} = 3.5$ GPa	$E_p^{f} = 230$ GPa	$E_p^{y} = 182.5$ GPa	$E_p^{y} = 180.15$ GPa
$w_1 = 0.96$ mm $w_2 = 1.10$ mm	$v^{m} = 0.35$	$E_t^{f} = 40$ GPa	$E_t^{y} = 18.5$ GPa	$E_t^{y} = 15.42$ GPa
$t_1 = 0.08$ mm $t_2 = 0.08$ mm		$G_{pt}^{f} = 24.0$ GPa	$G_{pt}^{y} = 7.55$ GPa	$G_{pt}^{y} = 6.574$ GPa
$t = 0.16$ mm		$v_{pt}^{f} = 0.26$	$v_{pt}^{y} = 0.28$	$v_{pt}^{y} = 0.2747$
		$G_{tt}^{f} = 14.3$ GPa	$G_{tt}^{y} = 6.70$ GPa	$G_{tt}^{y} = 5.494$ GPa
		$\beta^{y} = 0.78$		

Woven fabric composite data	[43] exper.	[43] anal.	This study CCA yarn model	This study FEA yarn model
E_1 [GPa]	49.3	52.4	55.97	54.65
E_2 [GPa]	60.3	58.9	62.22	60.74
G_{12} [GPa]	–	5.1	4.78	4.24
G_{13} [GPa]	–	–	2.98	2.81
G_{23} [GPa]	–	–	3.03	2.86
v_{12}	–	0.07	0.053	0.050
v_{13}	–	–	0.415	0.452
v_{23}	–	–	0.435	0.458
β	0.44		0.449	

Table 4. Comparison of this study results with those of [11] for e-glass/vinylester plain-weave composite laminate.

Matrix data	Yarn data	Geometric data
$E^{m} = 3.4$ GPa	$E_p^{y} = 57.5$ GPa	$w_i = s_i = 0.6$ mm
$\nu^{m} = 0.35$	$E_t^{y} = 18.8$ GPa	$t_i = 0.05$ mm
	$G_{pt}^{y} = 7.44$ GPa	$t = 0.10$ mm
	$\nu_{pt}^{y} = 0.25$	
	$\nu_{tt}^{y} = 0.29$	

Woven fabric composite data	[11] exper.	[11] anal.	This study
$E_1 = E_2$ [GPa]	24.8 ± 1.1	25.33	25.15
E_3 [GPa]	8.5 ± 2.6	13.46	10.47
G_{12} [GPa]	6.5 ± 0.8	5.19	5.038
$G_{13} = G_{23}$ [GPa]	4.2 ± 0.7	5.24	3.117
ν_{12}	0.1 ± 0.01	0.12	0.134
$\nu_{13} = \nu_{23}$	0.28 ± 0.07	0.29	0.341

Tables 2 and 3 show comparison of this study results with analytical and experimental results obtained by Naik and Ganesh [43]. They investigated single composite plies made of epoxy matrix and various types of fibres appearing in woven fabric yarns. Experimental data for only two longitudinal moduli were available for only two fibre types, e-glass and carbon, while approximate analytical method (slice array method) was used to also determine the in-plane shear modulus and in-plane Poisson ratio. Elastic properties and geometric parameters of the composite components used in the analysis are given in the upper part of both tables. Mechanical properties of yarns have been determined on the basis of fibre and matrix properties according to the analytical CCA method (results given after [43]) and the more exact FEA method,[44] for known fibre volume fraction β^{y}. Significant differences were only seen for yarns made of anisotropic carbon fibres. The lower parts of Tables 2 and 3 contain resulting composite material constants. As it can be seen, this study results are similar to the cited data, however, our stiffness moduli appear slightly higher than those reported in [43]. This can be explained by the fact that the cited data are obtained for a single layer, while this study model contains additional boundary conditions on the inter-layer common surface which make it stiffer.

Scida et al. [11] published results of similar computations performed for a plain-weave composite with the use of the CLT. They obtained analytically the full set of composite elastic constants, moreover, their computations were done for a multilayer laminate rather than for just a single layer. On the other hand, they limited themselves to only isotropic e-glass fibres in the composite microstructure (although the yarns, being fibre-matrix composite tows, were considered transversely isotropic). Elastic properties and geometric parameters of the composite components used in the analysis are given in the upper part of Table 4. The lower part of the table presents comparison of this study results with both analytical and experimental results of [11]. Again, this study results remain in satisfactory accordance with the experimental results, except for the G_{12} modulus which is underestimated (while the other cited analytical method visibly overestimates it).

4. Concluding remarks

The presented geometric model of RVE for plain-weave woven fabric features a number of important details that were neglected in previously published models. Constant yarn cross-section is preserved, even for highly undulated yarns. Yarn-to-yarn interface is modelled with all geometric details, including matrix-filled layer of variable thickness between intersecting yarns. Principal direction of transverse isotropy in yarns is locally aligned with fibre axis direction.

There are a few assumptions that may be questioned in the geometric definition of the model. One is sinusoidal shape of each fibre, i.e. a line corresponding to constant values of ξ_2 and ξ_3 in the parent configuration. It may be argued that these lines should consist of curved arches in the neighbourhood of actual contact zone with the intersecting yarn and straight segments between them. Such a concept, however, is based on the assumption that individual fibres have no stiffness for bending. Since this assumption is only approximately true, the assumed geometric simplification seems justified.

Another feature of the presented model that may be considered a drawback is different lengths of individual fibres crossing the yarn cross-sections at different locations. It can be seen that the edge line of the yarn is less undulated (and thus effectively shorter) than fibre lines in the centre of its width. However, these differences, also present in the very strict model of [30] seem justified as during the hot moulding process fibres have certain freedom of axial movement relative to their neighbours and such fibre length incompatibility can be accommodated this way.

The assumption $a_1 = \frac{1}{2}t_2$ and $a_2 = \frac{1}{2}t_1$ at $\xi_2 = 0$ ensures equal vertical coordinate x_3 at extreme warp and weft yarn surface bulges in the middle of the interlace zones ($x_1 = \pm s_2/2$, $x_2 = \pm s_1/2$). This condition may be questioned for yarn families with significant difference of yarn aspect ratio t_i/w_i. Thus, applicability of the presented model is limited to patterns in which $t_1/w_1 \approx t_2/w_2$. This approximation is reasonable in most actual composites.

Assumption of full adhesion in the interfaces between the microstructure constituents, made in the computational examples, may be criticized for its simplicity. It is stressed, however, that this was just the simplest choice and there is no difficulty to replace it by more advanced conditions, depending on nature of investigated phenomena. The finite element mesh generator ensures coincidence of surface nodes in meshes of yarns and matrix, but the contact conditions may be easily redefined as e.g. frictional slip. Besides, the matrix cushion in the yarn-to-yarn interface, that may require to be treated as separate material because of its actually observed porosity, is a separate part of the finite element mesh and may be thus easily assigned different material properties than those assumed for matrix. It is noteworthy that there is obviously no problem with assigning non-linear inelastic properties to all the microstructure constituents. These features indicate that presented model is in fact more universal than it has been shown in the numerical examples.

In spite of the mentioned simplifications, numerical examples show good agreement of the homogenized elastic constants of woven fabric composite with known experimental data.

It is concluded that this work establishes an enhanced basis for geometrical description of woven fabric composites. It is hoped that it will find applications in building advanced computational models of micro mechanical behaviour of composite materials.

Funding

This work received funding from the European Community's Seventh Framework Programme FP7/2007-2013 [grant agreement number 213371]; see http://www.maaximus.eu.

Notes

1. Strictly speaking, since the $\xi_1 = \pm 1$ sections of warp and weft yarns do not exactly lie in the planes $x_1 = \pm s_2$ or $x_2 = \pm s_1$, respectively, the RVE (understood as prismatic brick) will include some yarn points with the parent coordinate ξ_1 falling slightly beyond the interval $[-1, 1]$ while some other, with $\xi_1 \in [-1, 1]$, fall beyond the RVE domain. This is not a formal problem, though, as the transformation equations are well defined for any value of ξ_1.
2. For the sake of simplicity, we limit ourselves to present equations for only those yarns that interlace in the $x_1 > 0$, $x_2 > 0$ quarter of the RVE, i.e. those displayed in Figure 5(b). For the two other yarns the equations are analogous, only signs have to be reversed in appropriate places.
3. The case of external, upper or lower lamina in a multilayer section (whose one side deforms freely) is not considered here; if the number of layers is large enough, the expected inaccuracy caused by this negligence is assumed insignificant.

References

[1] Peng X, Cao J. A dual homogenization and finite element approach for material characterization of textile composites. Composites Part B 2002;33:45–56.
[2] Donadon MV, Falzon BG, Iannucci L, Hodgkinson JM. A 3-D micromechanical model for predicting the elastic behaviour of woven laminates. Compos. Sci. Technol. 2007;67:2467–2477.
[3] Komeili M, Milani AS. The effect of meso-level uncertainties on the mechanical response of woven fabric composites under axial loading. Comput. Struct. 2012;90–91:163–171.
[4] Gay D, Hoa SV, Tsai SW. Composite materials. Boca Raton (FL): CRC Press; 2002.
[5] Altenbach H, Altenbach JW, Kissing W. Mechanics of composite structural elements. Berlin: Springer-Verlag; 2004.
[6] Wisniewski K. Finite rotation shells. Basic equations and finite elements for Reissner kinematics. Barcelona: IMNE & Springer-Verlag; 2010.
[7] Ishikawa T, Chou T. Elastic behavior of woven hybrid composites. J. Compos. Mater. 1982;16:2–19.
[8] Ishikawa T, Chou T. One dimensional micromechanical analysis of woven fabric composites. AIAA J. 1983;21:1714–1721.
[9] Vandeurzen P, Ivens J, Verpoest I. A three-dimensional micromechanical analysis of woven-fabric composites: I. Geometric analysis. Compos. Sci. Technol. 1996;56:1303–1315.
[10] Vandeurzen P, Ivens J, Verpoest I. A three-dimensional micromechanical analysis of woven-fabric composites: II. Elastic analysis. Compos. Sci. Technol. 1996;56:1317–1327.
[11] Scida D, Aboura Z, Benzeggagh ML, Bocherens E. A micromechanics model for 3D elasticity and failure of woven-fibre composite materials. Compos. Sci. Technol. 1999;59:505–517.
[12] Aitharaju VR, Averill RC. Three-dimensional properties of woven-fabric composites. Compos. Sci. Technol. 1999;59:1901–1911.
[13] Bejan L, Poteraşu VF. Eigensensitivities for anisotropic materials with woven composite applications. Comput. Methods Appl. Mech. Eng. 2000;187:161–171.
[14] Carvelli V, Poggi C. A homogenization procedure for the numerical analysis of woven fabric composites. Composites Part A 2001;32:1425–1432.
[15] Rao MP, Pantiuk M, Charalambides PG. Modeling the geometry of satin weave fabric composites. J. Compos. Mater. 2009;43:19–56.
[16] Rao MP, Sankar BV, Subhash G. Effect of Z-yarns on the stiffness and strength of three-dimensional woven composites. Composites Part B 2009;40:540–551.
[17] Buchanan S, Grigorash A, Archer E, McIlhagger A, Quinn J, Stewart G. Analytical elastic stiffness model for 3D woven orthogonal interlock composites. Compos. Sci. Technol. 2010;70:1597–1604.

[18] Buchanan S, Grigorash A, Quinn JP, McIlhagger AT, Young C. Modelling the geometry of the repeat unit cell of three-dimensional weave architectures. J. Text. Inst 2010;101:679–685.
[19] Ansar M, Xinwei W, Chouwei Z. Modeling strategies of 3D woven composites: a review. Compos. Struct. 2011;93:1947–1963.
[20] Ivanov DS, Ivanov SG, Lomov SV, Verpoest I. Unit cell modelling of textile laminates with arbitrary inter-ply shifts. Compos. Sci. Technol. 2011;72:14–20.
[21] Lomov SV, Perie G, Ivanov D, Verpoest I. Modeling three-dimensional fabrics and three-dimensional reinforced composites: challenges and solutions. Text. Res. J. 2011;81:28–41.
[22] Nehme S, Hallal A, Fardoun F, Younes R, Hagege B, Aboura Z, Benzeggagh M, Chehade FH. Numerical/analytical methods to evaluate the mechanical behavior of interlock composites. J. Compos. Mater. 2011;45:1699–1716.
[23] Stig F, Hallström S. A modelling framework for composites containing 3D reinforcement. Compos. Struct. 2012;94:2895–2901.
[24] Hallal A, Younes R, Fardoun F. Review and comparative study of analytical modeling for the elastic properties of textile composites. Composites Part B 2013;50:22–31.
[25] Dasgupta A, Agarwal RK, Bhandarkar SM. Three-dimensional modeling of woven-fabric composites for effective thermo-mechanical and thermal properties. Compos. Sci. Technol. 1996;56:209–223.
[26] McBride TM, Chen J. Unit-cell geometry in plain-weave fabrics during shear deformations. Compos. Sci. Technol. 1997;57:345–351.
[27] Ito M, Chou T-W. Elastic moduli and stress field of plain-weave composites under tensile loading. Compos. Sci. Technol. 1997;57:787–800.
[28] Kuhn JL, Charalambides PG. Elastic response of porous matrix plain weave fabric composites: part i – modeling. J. Compos. Mater. 1998;32:1426–1471.
[29] Kuhn JL, Charalambides PG. Elastic response of porous matrix plain weave fabric composites: part II – results. J. Compos. Mater. 1998;32:1472–1507.
[30] Kuhn JL, Charalambides PG. Modeling of plain weave fabric composite geometry. J. Compos. Mater. 1999;33:188–220.
[31] Huang ZM. The mechanical properties of composites reinforced with woven and braided fabrics. Compos. Sci. Technol. 2000;60:479–498.
[32] Peng X, Cao J. A continuum mechanics-based non-orthogonal constitutive model for woven composite fabrics. Composites Part A 2005;36:859–874.
[33] Barbero EJ, Damiani TM, Trovillion J. Micromechanics of fabric reinforced composites with periodic microstructure. Int. J. Solids Struct. 2005;42:2489–2504.
[34] Onal L, Adanur S. Modeling of elastic, thermal, and strength/failure analysis of two-dimensional woven composites – a review. Appl. Mech. Rev. 2007;60:37–49.
[35] Glaessgen EH, Pastore CM, Griffin OH, Birger A. Geometrical and finite element modelling of textile composites. Composites Part B 1996;27:43–50.
[36] Sheng ZS, Hoa SV. Three-dimensional micro-mechanical modeling of woven fabric composites. J. Compos. Mater. 2001;35:1701–1729.
[37] Lin H, Clifford MJ, Long AC, Sherburn M. Finite element modelling of fabric shear. Modell. Simul. Mater. Sci. Eng. 2009;17:015008.
[38] Carrillo JG, Gamboa RA, Flores-Johnson EA, Gonzalez-Chi PI. Ballistic performance of thermoplastic composite laminates made from aramid woven fabric and polypropylene matrix. Polym. Test. 2012;31:512–519.
[39] Stoilova T, Lomov S. Round-robin formability study. Characterisation of glass/polypropylene fabric. Report. K.U. Leuven; 2004.
[40] Sherburn M. Geometric and mechanical modelling of textiles [PhD thesis]. Univ. Nottingham; 2007.
[41] Brown D, Morgan M, McIlhagger R. A system for the automatic generation of solid models of woven structures. Composites Part A 2003;34:511–515.
[42] ABAQUS 6.9. SIMULIA. Providence (RI USA); 2009.
[43] Naik NK, Ganesh VK. Prediction of on-axes elastic properties of plain weave fabric composites. Compos. Sci. Technol. 1992;45:135–152.
[44] Kowalczyk P. Parametric constitutive model of uni-directional fiber–matrix composite. Finite Elem. Anal. Des. 2012;50:243–254.